optica

Kramers–Kronig holographic imaging for high-space-bandwidth product: supplementary material

YOONSEOK BAEK,[1,2] KYEOREH LEE,[1,2] SEUNGWOO SHIN,[1,2] YONGKEUN PARK,[1,2,3,*]

[1]Department of Physics, Korea Advanced Institute of Science and Technology (KAIST), Daejeon 34141, South Korea
[2]KAIST Institute for Health Science and Technology, KAIST, Daejeon 34141, South Korea
[3]Tomocube, Inc., 48, Yuseong-daero 1184beon-gil, Yuseong-Gu, Daejeon 34051, South Korea
*Corresponding author: yk.park@kaist.ac.kr

Published 7 January 2019

This document provides supplementary information to "Kramers–Kronig holographc imaging for high-space-bandwidth product," https://doi.org/10.1364/OPTICA.6.000045. We describe detailed explanations about the analyticity condition and contour integration; discussions about discrete signals; the change in SBP depending on retrieval methods. Then we show experimental setups; simulation results to demonstrate minimum interferogram bandwidth; the effect of the zero-padding and strong reference on a complex amplitude image; a resolution comparison experiment. We also explain the methods for correcting aberration and phase artifacts. In addition, we show the off-axis complex amplitude image for the brain tissue and a MATLAB code for numerical simulation of the proposed method.

Derivation of Eq. (5)

From the definition of χ, we have $\chi(\mathbf{r})=\log[|1+\beta(\mathbf{r})|]+i\arg[1+\beta(\mathbf{r})]$. Then we get the following expressions for the real part.

$$\begin{aligned}\mathrm{Re}[\chi] &= \log\left[\left|1+\beta\right|\right] \\ &= \log\left[\left|1+\frac{S}{R}\right|\right] \\ &= \frac{1}{2}\log\left[\left|\frac{S+R}{R}\right|^2\right] \\ &= \frac{1}{2}\left[\log\left|S+R\right|^2-\log|R|^2\right].\end{aligned} \tag{S1}$$

Note that the last equality of Eq. (S1) is identical to Eq. (5a). The imaginary part of χ is simply $\arg[1+\beta(\mathbf{r})]$ identical to Eq. (5b).

2D analyticity of χ and contour integration

In the main text, Eq. (8) is derived based on the one-dimensional (1D) analyticity condition. In this section, we show that Eq. (8) of the main text guarantees the analyticity of a two-dimensional (2D) function. The 1D analyticity condition in Eq. (8) can be extended to a 2D condition with an additional condition [1],

$$\tilde{\chi}\left(\nu_{\parallel}=0,\nu_{\perp}\right)=0, \tag{S2}$$

where $\tilde{\chi}(\mathbf{v})$ is the 2D Fourier transform of $\chi(\mathbf{r})$ and $\mathbf{v}=\nu_{\parallel}\hat{\mathbf{v}}_{\parallel}+\nu_{\perp}\hat{\mathbf{v}}_{\perp}$ with $\mathbf{v}_{\perp}\cdot\mathbf{v}_{R}=0$. Thus for a 2D function χ to be analytic Eq. (8) and Eq. (S2) must be satisfied at the same time. Since χ is a power series of β [see Eq. (6)], Eq. (S2) can be replaced with the following condition for all positive integer n,

$$\mathcal{F}[\beta^n]\left(\nu_{\parallel}=0,\nu_{\perp}\right)=0, \tag{S3}$$

where $\mathcal{F}[h]$ indicates the 2D Fourier transformation of a function h. Here it should be noted that $\beta(\mathbf{r})$ is a band-limited function [Eq. (7)]. Therefore, when Eq. (8) is satisfied, $\tilde{\beta}(\mathbf{v})$ is supported only in the positive frequency domain of $\nu_{\parallel}$ satisfying Eq. (S3) for n = 1. Same is true for higher orders; β^n is a band-limited function whose Fourier spectrum is supported only in the positive frequency of $\nu_{\parallel}$. Therefore Eq. (8) becomes a sufficient condition of Eq. (S2). Moreover, the validity of the KK relations is guaranteed only by Eq. (8). To retrieve a complex amplitude image the contour integration in Eq. (4) must be conducted. For a 1D function, it is known that the contour integration can be replaced with the 1D Hilbert transform. Since we adopted the 2D analyticity based on the directional Hilbert transform [1], the contour integration can be conducted as

$$\mathrm{Im}\left[\chi(\mathbf{r})\right]=-i\mathcal{F}^{-1}\left[\mathcal{F}\left[\mathrm{Re}(\chi)\right](\mathbf{v})\times\mathrm{sgn}\left(\mathbf{v}\cdot\hat{\mathbf{v}}_{\parallel}\right)\right], \tag{S4}$$

where $\mathcal{F}^{-1}[h]$ is the inverse 2D Fourier transform of a function h, and sgn is a signum function whose value is determined by the inner product between $\mathbf{v}$ and $\hat{\mathbf{v}}_{\parallel}$.

Analyticity and contour integration of discrete signal

To describe the working principle of the proposed method, we assumed $S(\mathbf{r})$, $R(\mathbf{r})$ and $\chi(\mathbf{r})$ to be continuous functions. Since they are related to complex amplitudes of lights, they exists as a continuous signal. The issue might occur when we discretely sample them. However a properly sampled signal can reconstruct the continuous signal according to Nyquist-Shannon sampling theorem [2] and Whittaker-Shannon interpolation theorem [3]. This is why the proposed method requires sufficient zero-padding to the measured interferograms, which guarantees discrete signals to follow the logic of the continuous signals.

The computation of the KK relations are based on analytic-like discrete signal [4]. Such a signal should satisfy the discrete version of Eq. (8). For example in the case $\hat{\mathbf{v}}_{\parallel} = \hat{\mathbf{v}}_x$, we have

$$|\mathbf{v}_R| \geq \frac{\mathrm{NA}_{\mathrm{obj}}}{\lambda M} + \frac{1}{N\Delta x}, \qquad \textbf{(S5)}$$

where N is the pixel count in x-direction and Δx is the size of pixel. The real and imaginary part of the analytic-like discrete signal is related by the Eq. (S4) described with discrete Fourier transforms. Technically speaking, the use of discrete Fourier transform for the computation of Eq. (S4) requires special care at the minimum spatial frequency component for an even-numbered discrete signal. Unlike the case of the continuous signal, the signum function should be zero at the minimum spatial frequency. This is because the minimum frequency shares the boundary with the repeated signal spectrums [4]. Thus the contour integration in Eq. (S4) can be computed using discrete Fourier transform with a modified signum function;

$$\mathrm{sgn}\left(\frac{n}{N\Delta x}\right) = \begin{cases} 0 & \text{if } n = 0, \\ -1 & \text{if } 1 \leq n < N/2-1, \\ 0 & \text{if } n = N/2, \\ 1 & \text{if } N/2+1 \leq n < N-1. \end{cases} \qquad \textbf{(S6)}$$

It should be noted that the modification at the boundary becomes less important as the size of the zero-padding increases, because χ is a decaying function in the frequency domain (see supplement section titled Handling Nonlinear Operation).

Change in SBP depending on modulation directions and retrieval methods

SBP of the complex amplitude varies depending on the retrieval method and the modulation direction of a reference beam. As a comparison, Fourier spectrums of interferograms in different cases are shown in Fig. S1. In the figure, $\widetilde{B}(\mathbf{v}-\mathbf{v}_R)$ and $\widetilde{B}^*(-\mathbf{v}-\mathbf{v}_R)$ are indicated with green and $\widetilde{A}(\mathbf{v})$ is indicated with gray.

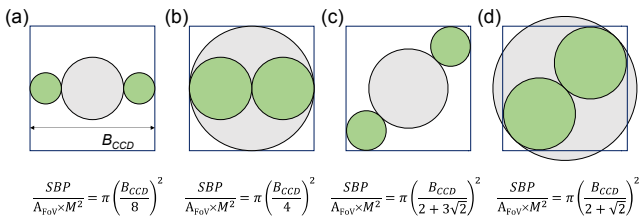

Fig. S1. Change in SBP depending on modulation directions and retrieval methods. A_{FoV} is the area of an image at the sample plane and M indicates the total magnification. Fourier spectra of horizontally modulated off-axis interferograms (a) for the conventional method and (b) for the proposed method. Fourier spectra of diagonally modulated off-axis interferograms (c) for the conventional method and (d) for the proposed method. The proposed method shows 4-fold and 3.34-fold increases in the SBP for the horizontal modulation [(a) and (b)], and the diagonal modulation [(c) and (d)], respectively.

We assumed a detector bandwidth, or the inverse of a pixel pitch, to be B_{CCD}. In addition, we assumed a case where a detector pixel count becomes a bottleneck to SBPs. Thus the size of the image at the detector ($A_{FoV}\times M^2$) is identical to the size of the detector and considered to be a constant. Figure S1(a) shows the Fourier spectrum of an interferogram when a horizontally modulated reference beam and the conventional off-axis method are adopted. The SBP of the first-order term is proportional to $(B_{CCD}/8)^2$. Fig. S1(b) shows the Fourier spectrum of an interferogram when a horizontally modulated reference beam and the proposed method are adopted. The SBP of the first-order term is proportional to $(B_{CCD}/4)^2$, which is a 4-fold increase compared to the case of Fig. S1(a).

Figure S1(c) is the case when a diagonally modulated reference beam and the conventional off-axis method are considered. The SBP of the first-order term is proportional to $(B_{CCD}/(2+3\sqrt{2}))^2$. Figure S1(d) is the case with a diagonally modulated reference beam and the proposed method. The SBP of the first-order term is proportional to $(B_{CCD}/(2+\sqrt{2}))^2$, which is a 3.34-fold increase compared to the case of Fig. S1(c).

Experimental Setup

The experimental setup is shown in Fig. S2. The setup is a Mach-Zehnder interferometer with a HeNe laser (λ = 632.8 nm, HRR050, Thorlabs, New Jersey, USA). A collimated beam from the laser is split by a polarizing beam splitter (PBS); one arm illuminates a sample while the other acts as a reference beam. Two beams are combined by another PBS in front of a camera (MQ042MG-CM, XIMEA, Münster, Germany for the imaging of a 1951 USAF resolution target and polystyrene beads; MD120MU-SY, XIMEA, Münster, Germany for the imaging of human breast tissue and mouse brain tissue). The reference beam is slightly tilted with respect to the propagation direction of the sample beam to generate off-axis interferograms.

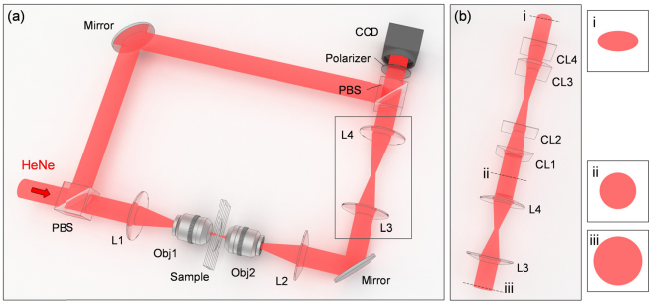

Fig. S2. Experimental setup. (a) The experimental setup is based on an off-axis Mach-Zehnder interferometer. L: lens; Obj: objective lens; PBS: polarizing beam splitter. (b) When an anamorphic imaging is adopted, a part of the setup is changed; anamorphic 4-f arrays of cylindrical lenses (CL1-CL4) are added after the 4-f array of L3 and L4. Images at the right shows shapes of beams at different positions of the setup.

Depending on samples, we employed different condenser lenses (LMPLFL N 50X, Olympus, Tokyo, Japan for the USAF resolution target and polystyrene beads; UPLFLN 10X2, Olympus, Tokyo, Japan for the human breast tissue; PLN 4X Olympus, Tokyo, Japan for the mouse brain tissue) and objective lenses (UPLSAPO 60XW for the USAF resolution target and polystyrene beads, and UPLSAPO 10X2, Olympus, Tokyo, Japan for the human breast tissue and the mouse brain tissue). The focal length of L1 and L2 are 200 mm and 180 mm respectively. The additional lenses L3 and L4 are placed in a 4-*f* geometry, to adjust the total magnification of the microscopic system. The focal lengths of L3 and L4 vary depending on the experiment. When imaging the USAF resolution target and polystyrene beads, the focal lengths of L3 and L4 are 60 mm and 150 mm respectively. When imaging a breast tissue, the focal lengths of L3 and L4 are changed to 200 mm identically. When imaging a brain tissue, 4 cylindrical lenses are added after the 4-*f* system of L3 and L4, to maximize the available SBP [Fig. S2(b)]. The power axes of CL1 and CL3 are horizontal to the floor and the power axes of CL2 and CL4 are vertical to the floor. The focal lengths of L3 and L4 are 150 and 125 mm. The focal length of CL1-CL4 are 300, 400, 300 and 200 mm respectively. CL1 and CL3 forms a 4-*f* relay whose magnification is 1 in the horizontal axis. CL2 and CL4 forms a 4-*f* relay whose magnification is 1/2 in the vertical axis.

Minimum bandwidth for KK holographic imaging

The minimum bandwidth for the conventional off-axis method and that for the proposed method are compared in Fig. S3. $\widetilde{B}(\mathbf{v}-\mathbf{v}_R)$ and $\widetilde{B}^*(-\mathbf{v}-\mathbf{v}_R)$ are indicated with green color and $\widetilde{A}(\mathbf{v})$ is indicated with gray color. In the conventional off-axis method, the required bandwidth in the modulation direction is $8\mathrm{NA}_{\mathrm{obj}}/\lambda M$, and that in the perpendicular direction is $2\mathrm{NA}_{\mathrm{obj}}/\lambda M$ [Fig. S3(a)]. Since the conventional off-axis method is based on the direct filtering in the frequency domain, the required minimum bandwidth is straightforward. In the proposed method, the required bandwidth in the modulation direction is $4\mathrm{NA}_{\mathrm{obj}}/\lambda M$, which is determined by the analyticity condition. The required bandwidth in the perpendicular direction is $2\mathrm{NA}_{\mathrm{obj}}/\lambda M$. This is because the proposed method utilizes the KK relations along the modulation direction and not in the direction perpendicular to the modulation.

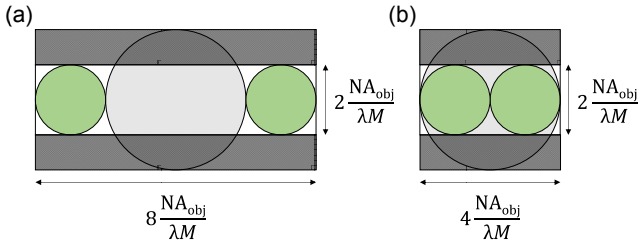

Fig. S3. Minimum bandwidths for two field retrieval methods (a) Fourier spectrum of the off-axis interferogram in the case of the conventional off-axis method. The minimum bandwidth in the modulation direction is $8\mathrm{NA}_{\mathrm{obj}}/\lambda M$. And that in the direction perpendicular to the modulation is $2\mathrm{NA}_{\mathrm{obj}}/\lambda M$. (b) Fourier spectrum of the off-axis interferogram in the case of the proposed method. The minimum bandwidth in the modulation direction is $4\mathrm{NA}_{\mathrm{obj}}/\lambda M$., and that in the direction perpendicular to the modulation is $2\mathrm{NA}_{\mathrm{obj}}/\lambda M$.

To demonstrate the minimum bandwidth for the proposed method, we performed a simulation under different bandwidths. In Fig. S4, the upper row corresponds to the oversampled condition, and the bottom row corresponds to the minimum bandwidth condition. In the simulation, a sample beam has a circular pupil function and a reference beam whose amplitude is 1.1 times the maximum amplitude of the sample beam is used. During the retrieval process, interferograms are zero-padded to triple the bandwidth along the modulation direction, while its bandwidth along the perpendicular direction remains unchanged.

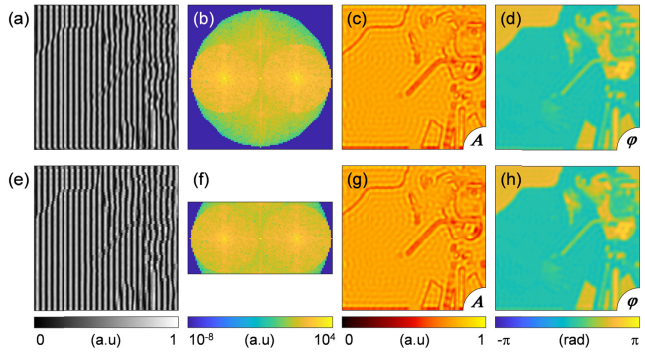

Fig. S4. Comparison between different bandwidth conditions for the proposed method. (a) An off-axis interferogram oversampled in the direction perpendicular to the modulation. (b) The Fourier spectrum of (a). (c-d) Retrieved amplitude and phase using (a). (e) An off-axis interferogram at the minimum bandwidth condition. (f) The Fourier spectrum of (e). (g-h) Retrieved amplitude and phase using (e).

Fig. S4(a) is the interferogram sampled with the bandwidths of $4\mathrm{NA}_{\mathrm{obj}}/\lambda M$ in both directions. Fig. S4(b) is the Fourier spectrum of the interferogram. Fig. S4(c-d) shows the retrieved complex amplitude using the proposed method. The cross-correlation of the retrieved field with the sample field is exactly 1. Fig. S4(e) is the interferogram sampled with the minimum bandwidth Fig. S4(f) is the Fourier spectrum of the interferogram. Fig. 4(g-h) shows the retrieved complex amplitude. The cross-correlation of the retrieved field with the sample field is again exactly 1. This result shows that the proposed method requires a bandwidth of $2\mathrm{NA}_{\mathrm{obj}}/\lambda M$ in the perpendicular direction and $4\mathrm{NA}_{\mathrm{obj}}/\lambda M$ in the modulation direction.

Handling Nonlinear Operation

The proposed method involves a nonlinear operation, a logarithm, which expands the bandwidth of a signal. In practice, this can affect the validity of the KK relations because of aliasing. The effect of the nonlinear operation can be found in the 1D Fourier transform of χ,

$$\mathcal{F}_{r_\parallel}[\chi](\nu_\parallel,r_\perp)=\mathcal{F}_{r_\parallel}[\beta](\nu_\parallel,r_\perp)+\sum_{n=1}^{\infty}\frac{(-1)^n}{n+1}\left[M^{n+1}\left(\mathcal{F}_{r_\parallel}[\beta](\nu_\parallel,r_\perp)\right)\right], \quad \textbf{(S7)}$$

where $\mathcal{F}_{r_\parallel}[h]$ is a 1D Fourier transform of a function h about $r_\parallel$, and $M^n[h]$ indicates the n-th order convolution of h ($n \geq 2$) defined as $M^n[h]=\underbrace{h*\cdots*h}_{n\ \text{times}}$ where $*$ indicates the convolution with respect to $\nu_\parallel$. Note that $M^n[h]$ results in an n-fold increase in the bandwidth, and translation of the spectrum. Thus, for χ satisfying the analytic condition in Eq. (8), its Fourier spectrum reaches from zero to positive infinity of $\nu_\parallel$. The aliasing of high order convolutions occurs when the bandwidth of an image sensor is finite. Due to the

aliasing, high-frequency components of χ appear in the negative frequency domain. This affects the validity of the KK relations resulting noise in the retrieved complex amplitude using the proposed method.

To minimize the unwanted effect of the aliasing, two methods are proposed. The first method is zero-padding. The interferogram and the image of the reference beam are zero-padded in their frequency space before taking the logarithm according to Eq. (5a). This increases the numerical bandwidth, which can effectively resolve the aliasing of high order convolution terms in Re(χ). It should be emphasized that the zero-padding is required only in the modulation direction $v_{\parallel}$. It should be noted that, a constant factor should be multiplied to compensate the decrease in values allocated to pixels as a result of the zero-padding.

The second method is to keep the intensity of the reference beam stronger than the intensity of the sample beam. This ensures convolution terms to rapidly decay in its amplitude as the convolution order increases. Since the two methods treat an identical issue, one can keep the intensity of the reference beam comparable to that of the sample beam simply by increasing the size of zero-padding. In the experiments, we employed both methods. Images are zero-padded in the frequency space to triple bandwidths of images in the modulation direction $v_{\parallel}$, and the intensity of the reference beam was kept two times stronger than that of the sample beam; $|R|^2 \sim 2|S|^2$.

Effect of zero-padding and strong reference

In this section, we demonstrate how two methods affect the retrieved complex amplitude. We conducted a simulation in three different cases; (1) weak reference, without zero-padding (2) weak reference, with zero-padding (3) strong reference, without zero-padding, Fig. S5 shows the results. In all three cases, sample beams with circular pupil functions are used.

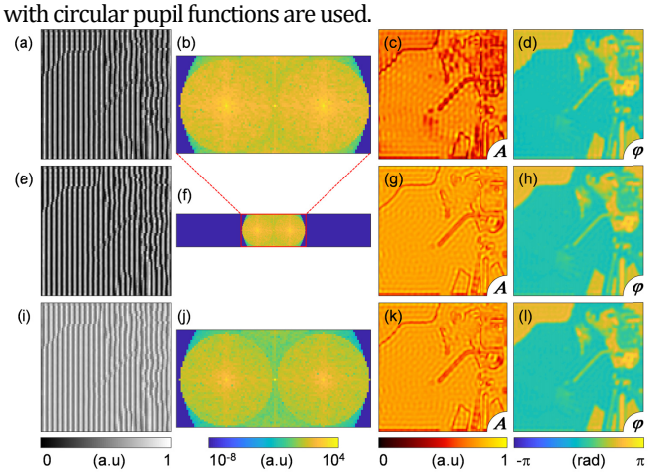

Fig. S5. Effect of zero-padding and strong reference. (a) A non-zero-padded off-axis interferogram measured with a weak reference. (b) Fourier spectrum of (a). (c-d) Retrieved amplitude and phase from (a). (e) A zero-padded off-axis interferogram measured with a weak reference. (f) Fourier spectrum of (e). (g-h) Retrieved amplitude and phase from (e). (i) A non-zero-padded off-axis interferogram measured with a strong reference. The interferogram is not zero-padded. (j) Fourier spectrum of (i). (k-l) Retrieved amplitude and phase from (i).

The upper row is the simulation results with a reference beam whose amplitude is 1.1 times the maximum amplitude of the sample beam. Here zero-padding is not used. Fig. S5(a) shows the simulated off-axis interferogram. Fig. S5(b) is the Fourier spectrum of the interferogram. Fig. S5(c)-(d) shows the complex amplitude retrieved from Fig. S5(a). The cross-correlation with the actual sample beam is 0.9729. Due to the limited bandwidth, the function χ is not correctly expressed, resulting in an incorrect retrieval of the complex amplitude.

The middle row is the results with the same reference and zero-padding. Fig. S5(e) shows the zero-padded interferogram. The interferogram is zero-padded in the frequency domain to triple the size in the modulation direction [Fig. S5(f)]. Fig. S5(g)-(h) show the retrieved complex amplitude from Fig. S5(e). The cross-correlation with the actual sample beam is exactly 1. The result shows that the zero-padding enables a correct retrieval of the complex amplitude for a weak reference. A sample beam with strong high-order convolution terms may necessitate larger size of zero-padding to retrieve a correct complex amplitude.

The bottom row is the results with a strong reference whose amplitude is four times the maximum amplitude of the sample beam. Zero-padding is not used. Fig. S5(i) shows the corresponding interferogram. Fig. S5(j) is the Fourier spectrum of the interferogram. Fig. S5(k-l) shows the retrieved complex amplitude. The cross-correlation with the actual sample beam is 0.9978. The strong reference gives a similar effect to the zero-padding. The stronger the reference is, the higher cross-correlation is obtained.

Resolution comparison at the same bandwidth

The proposed method enables high SBP imaging than the conventional off-axis method for a given detector bandwidth. Thus it can utilize a large pupil function to provide a wide FoV or a high resolution. In this section, we demonstrate resolution comparison between the proposed method and the conventional off-axis methods at the same lateral bandwidth.

The experimental setup is identical to Fig. S2(a). We adopted a condenser lens (0.7 NA, LUCPLFL N 60X, Olympus, Tokyo, Japan) and an imaging objective lens (0.5 NA, LMPLFL N 50X, Olympus, Tokyo, Japan). The focal lengths of L3 and L4 are 150 and 125 mm, respectively. For a sample a 1951 USAF resolution target is used. To control the size of the pupil function while keeping the total magnification and the FoV, we placed a circular aperture at the Fourier plane of the image located between L3 and L4.

The experimental result is shown in Fig. S6. The top row shows the result of the proposed method including retrieved complex amplitude image and the Fourier spectrum of the interferogram. The bottom row shows the result of the conventional off-axis method. At the same lateral bandwidth of 0.076 μm^{-1}, the proposed method can utilize the full NA (0.5) of the objective lens. On the contrary, the conventional off-axis method sacrifices the NA (0.25) to ensure signal isolation in the frequency space.

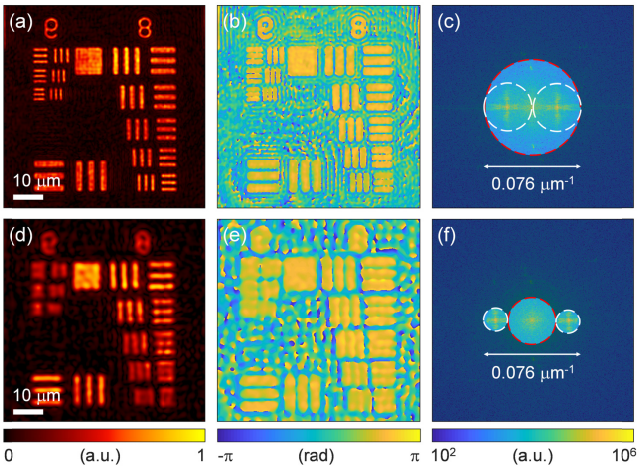

Fig. S6. Resolution comparison at the same bandwidth. (a) Amplitude and (b) phase image obtained using the proposed method. (c) Fourier spectrum of the interferogram used to retrieve (a) and (b). (d) Amplitude and (e) phase obtained using the conventional off-axis method. (f) Fourier spectrum of the interferogram used to retrieve (d) and (e).

Aberration correction

When cylindrical lenses are adapted to perform imaging, aberration can arise due to the optical path difference (OPD) between lights passing different positions of cylindrical lenses. When two sets of cylindrical 4-*f* imaging systems that are perpendicular to each other as in Fig. S2(b) are used, an optical field in the vertical direction (parallel to power axis of CL2 and CL4) and that in the horizontal direction (parallel to power axis of CL1 and CL3) undergo different phase delays, which results in aberration.

To be specific, the optical field at the sample plane, $E(x,y)$, measured by the imaging system can be described as

$$E(x,y)=\mathcal{F}^{-1}\left[\widetilde{E}_0(\nu_x,\nu_y)\times e^{2\pi i\{Q_y(\nu_y)+Q_x(\nu_x)\}}\right],$$
$$Q_y(\nu_y)=t_{\mathrm{CL1}}\left[\sqrt{n^2\nu_0^2-\nu_y^2}-\sqrt{\nu_0^2-\nu_y^2}\right], \quad \textbf{(S8)}$$
$$Q_x(\nu_x)=t_{\mathrm{CL4}}\left[\sqrt{n^2\nu_0^2-(\nu_x/M_x)^2}-\sqrt{\nu_0^2-(\nu_x/M_x)^2}\right],$$

where $\mathcal{F}^{-1}$ indicates the inverse 2D Fourier transform; $\widetilde{E}_0(\nu_x,\nu_y)$ is the Fourier transform of the aberration-free optical field at the sample plane; Q_y and Q_x describes the phase delay induced by the cylindrical lenses in each direction; n is the refractive index of cylindrical lenses; $t_{\mathrm{CL}i}$ is the central thickness of a cylindrical lens CL*i*; the cutoff frequency ν_0 is $1/\lambda$; M_x indicates a magnification in the *x*-direction (parallel to power axes of CL1 and CL3). In Eq. (S8), Q_y describes the phase delay induced by the CL1 that affects the imaging in the *y*-direction by CL2 and CL3. Since the CL1 is placed at the sample plane, the effect of magnification is not included in Q_y. Similarly, Q_x describes the phase delay induced by CL4 to the imaging in the *x*-direction by CL1 and CL3. Unlike the case of CL1, CL4 is placed after the 4-*f* array. Thus the effect of CL4 is applied to the (de)magnified image, which makes Q_x be dependent on the magnification, M_x. It should be noted that the effect of CL2 and CL3 is neglected, because it can be compensated by adjusting the distance between lenses in 4-*f* arrays.

Thus the aberration can be corrected by compensating the exponential terms in Eq. (S8) as

$$E_0(x,y)=\mathcal{F}^{-1}\left[\widetilde{E}(\nu_x,\nu_y)\times e^{-2\pi i\{Q_y(\nu_y)+Q_x(\nu_x)\}}\right], \quad \textbf{(S9)}$$

where $\widetilde{E}(\nu_x,\nu_y)$ is the Fourier transform of the measured optical field at the sample plane. In the experiment, the magnification in the *x*-direction is one (M_x =1). The refractive indexes of cylindrical lenses are 1.5151 at 632.8 nm, and a central thickness of CL1 and CL4 are 5.9 and 4.1 mm respectively.

Artifact removal in wide field-of-view imaging

The quantitative phase image in Fig. 4(a) of the main text shows an artifact in the phase induced by the thickness variation of coverslips. For this, we isolated the artifact from the sample information. First, the measured optical field is low-pass filtered with a cutoff spatial frequency corresponding to an NA of 0.004 to extract features larger than 92 μm. Since the sample exhibits features much smaller than the artifact, the low-pass filtering provides a good approximation of the artifact [5]. Then the phase of the artifact is subtracted from the phase of the sample. As a result, artifact in the quantitative phase image is removed [Fig. 4(b)].

In general, the low-pass filtering method eliminates low-spatial frequency information of the sample. However this is not the case, since structural features of the sample have high-spatial frequencies that are not affected by the method. The method described above sets the phase of the background region located at the center of Fig. 4(a). This is because the background region has a large structure comparable to the artifact. Thus the phase of the background region is corrected by adding the average phase values of other small background regions.

Complex amplitude image of the brain tissue using the conventional off-axis method

In this section we show the retrieved complex amplitude of the brain tissue shown in Fig. 4 using the conventional off-axis method. In Fig. S7, the retrieved and the corrected quantitative phase image are shown. The noise induced by the spectral overlap can be observed in the enlarged images of Fig. S7(b). The noise has high spatial frequencies, because the effect of the autocorrelation term mainly appears at the boundary of the pupil function. They are contrasted with the image retrieved by the proposed method [Fig. S7(c-d)], which provide clear images without the noise fount in the conventional off-axis method.

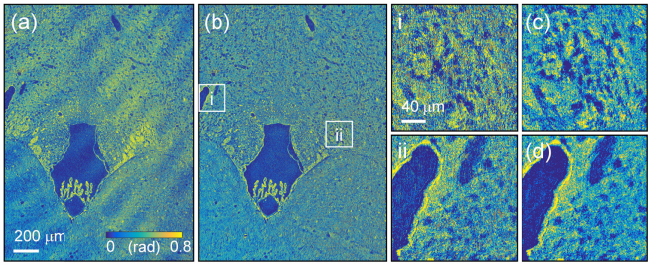

Fig. S7. (a) The quantitative phase image of the brain tissue retrieved using the conventional off-axis method (b) The correct image of (a) where the multiple reflections induced by the coverslips are removed. Enlarged images of different positions (i, ii) are shown. (c-d) The enlarged images retrieved with the proposed method at the same positions (i, ii).

MATLAB code for the numerical simulation

The following is a MATLAB code for the numerical simulation of the proposed method with two different complex amplitude image. It uses two images provided by MATLAB; autumn.tif and cameraman.tif. Instead one can also use a cosine amplitude pattern for simulation. In the simulation, an ideal plane wave reference is assumed. In addition the spatial frequency of the reference beam lies in negative ν_x domain for the simplicity in computing the contour integration. The simulation is conducted at the minimum bandwidth condition of the provided method as shown in Fig. S4(f). After running this code, it will show three result; (1) exact complex amplitudes of a sample beam, (2) complex amplitudes obtained from the proposed method and (3) complex amplitudes obtained from the off-axis method. It also prints $g^{(1)}$ correlations of the retrieved complex amplitudes with the exact values.

```
% MATLAB code for the numerical simulation of KK holography
% written by YoonSeok Baek, 2018-11-06
clear
flag = 0;
%% define a sample field
%% (1) autumn amplitude & cameraman phase
image_size = 160; % number of pixels in one direction;
offset = 20; % offset for cropping image
amplitude_image = double(imread('autumn.tif'));
amplitude_image = amplitude_image(offset+1:offset+image_size,
offset+1:offset+image_size);
amplitude_imgae = amplitude_image./max(amplitude_image(:));

phase_image = double(imread('cameraman.tif'));
phase_image =
phase_image(offset+1:offset+image_size,offset+1:offset+image_siz
e);
phase_image = -phase_image./max(phase_image(:))*pi+2;
sample_field = amplitude_image.*exp(1i*phase_image);

%% (2) Cosine pattern
% image_size = 60; % number of pixels in one direction; also
becomes a number of pixels in detector bandwidth
% sample_field_Fourier = zeros(image_size,image_size);
% sample_field_Fourier(floor(image_size/2+1)-
6,floor(image_size/2+1)-6) = 1;
%
sample_field_Fourier(floor(image_size/2+1),floor(image_size/2+1
)) = 3;
%
sample_field_Fourier(floor(image_size/2+1)+6,floor(image_size/2
+1)+6) = 1;
% sample_field = fftshift(ifft2(ifftshift(sample_field_Fourier)));
% flag = 1;

%% define a pupil function
% the radius of a pupil function
% below is the maximum possible radius for a given detector
bandwidth
pupil_radius = round(image_size/4)-1;

% create the circular pupil with a raidus of 'pupil_radius'
[x_array,y_array] = meshgrid(1:image_size,1:image_size);
x_array = x_array - floor(max(x_array(:))/2+1); % center of image
to be zero
y_array = y_array - floor(max(y_array(:))/2+1); % center of image
to be zero
pupil_function =
(x_array./pupil_radius).^2+(y_array./pupil_radius).^2 <= 1;

%% create a band-limited signal with a circular pupil
sample_field_Fourier = fftshift(fft2(ifftshift(sample_field)));
sample_field_Fourier = sample_field_Fourier.*pupil_function;

% generated band-limited sample field
sample_field = fftshift(ifft2(ifftshift(sample_field_Fourier)));

% normalize maximum amplitude to 1 for simplicity
sample_field = sample_field./max(abs(sample_field(:)));
sample_field_Fourier = fftshift(fft2(ifftshift(sample_field)));

%% define a reference field (tilted plane wave)
% create an off-axis plane wave reference field
ref_field_Fourier = zeros(image_size,image_size);
ref_spatial_freq = -1*(ceil(pupil_radius)+1);
% add one to satisfy the analyticity condition
% negative one is multiplied for the simplicity in using matlab
function 'hilbert'
ref_field_Fourier(floor(image_size/2+1),floor(image_size/2+1)+ref
_spatial_freq) =
max(abs(sample_field(:)))*length(sample_field(:))*2;
% spatial modulation of the reference beam in x-direction
% its amplitude is twice the maximum amplitude of the sample
beam
ref_field = fftshift(ifft2(ifftshift(ref_field_Fourier)));

%% create an off-axis interferogram
net_field = sample_field + ref_field;
interferogram = abs(net_field).^2;

% interferogram normalized with reference beam intensity image
interferogram = interferogram./abs(ref_field).^2;

% down-sample the interferogram along y-axis to demonstrate
minimum bandwidth condition for the proposed method
% see Fig.S4(f)
interferogram_down_sampled = downsample(interferogram,2);
interferogram_down_sampled_Fourier =
fftshift(fft2(ifftshift(interferogram_down_sampled)));

% zero padding interferograms in Foureir space
% higher value required for strong high-order convolutions

if flag
   zero_pad_const = 4;
    % more zero-padding required for the cosine pattern
else
   zero_pad_const = 2;
end

normalization_const1 =
length(interferogram_down_sampled_Fourier(:)); %
normalization constant for zero-padding
interferogram_down_sampled_Fourier =
padarray(interferogram_down_sampled_Fourier,[0,image_size*ze
ro_pad_const],'both');
normalization_const2 =
length(interferogram_down_sampled_Fourier(:));% normalization
constant for zero-padding
interferogram_down_sampled_Fourier =
interferogram_down_sampled_Fourier/normalization_const1*nor
malization_const2; % normalization to mimic high sampling rate
```

```
interferogram_down_sampled =
fftshift(ifft2(ifftshift(interferogram_down_sampled_Fourier)));

%% Retrieval of KK sample field
% take log of interferogram according to Eq.(5)
log_interferogram_down_sampled =
log(interferogram_down_sampled);
[size_y,size_x] = size(log_interferogram_down_sampled);

% apply KK relations to obtain amplitude and phase of S/R
kk_real_part = log_interferogram_down_sampled./2; %
(1/2)*log(|1+S/R|)^2 = log(abs(E_kk))
kk_imaginary_part = imag(hilbert(real(kk_real_part).')).'; % for this
simulation the contour integration is hilbert transform about x
kk_sample_field = exp(kk_real_part+1i*kk_imaginary_part)-1; %
exp(log(S/R+1))-1 = S/R

% remove the zero padding to match the size with the answer
kk_sample_field_Fourier = fftshift(fft2(ifftshift(kk_sample_field)));
kk_sample_field_Fourier = circshift(kk_sample_field_Fourier,[0,-
image_size*zero_pad_const]);
kk_sample_field_Fourier = kk_sample_field_Fourier(:,1:image_size);
kk_sample_field = fftshift(ifft2(ifftshift(kk_sample_field_Fourier)));
kk_sample_field = kk_sample_field.*downsample(ref_field,2);

% upsample in the vertical direction to match the size with the
answer
kk_sample_field_Fourier = fftshift(fft2(ifftshift(kk_sample_field)));
kk_sample_field_Fourier =
padarray(kk_sample_field_Fourier,[(image_size-
size_y)/2,0],'both');
% apply pupil function for possible aliasing artifacts
kk_sample_field_Fourier =
kk_sample_field_Fourier.*pupil_function;
kk_sample_field = fftshift(ifft2(ifftshift(kk_sample_field_Fourier)));
kk_sample_field = kk_sample_field./max(abs(kk_sample_field(:)));

%% Retrieval using the conventional off-axis method
interferogram = abs(net_field).^2;
interferogram_down_sampled2 = downsample(interferogram,2);
interferogram_down_sampled_Fourier2 =
fftshift(fft2(ifftshift(interferogram_down_sampled2)));

ox_sample_field_Fourier =
circshift(interferogram_down_sampled_Fourier2,[0,ref_spatial_fre
q]).*pupil_function(image_size/4+1:end-image_size/4,:);
ox_sample_field_Fourier =
padarray(ox_sample_field_Fourier,[image_size/4,0],'both');
ox_sample_field = fftshift(ifft2(ifftshift(ox_sample_field_Fourier)));
ox_sample_field = ox_sample_field./max(abs(ox_sample_field(:)));

%% Display result
figure(1),
subplot(3,3,1),
imagesc(abs(sample_field),[0,max(abs(sample_field(:)))]), axis
image, axis off, title('Sample amplitude'), colorbar
subplot(3,3,2), imagesc(angle(sample_field),[-pi,pi]), axis image,
axis off, title('Sample phase'), colorbar
subplot(3,3,3), imagesc(log10(abs(sample_field_Fourier)),[-
4,max(log10(abs(sample_field_Fourier(:))))]), axis image, axis off,
title('Fourier spectrum (log_1_0)'), colorbar
% subplot(3,3,3), imagesc((abs(sample_field_Fourier))), axis
image, axis off, title('Fourier spectrum'), colorbar
subplot(3,3,4),
imagesc(abs(kk_sample_field),[0,max(abs(kk_sample_field(:)))]),
axis image, colorbar, title('KK amplitude'), axis off
subplot(3,3,5), imagesc((angle(kk_sample_field)),[-pi,pi]), axis
image, colorbar, title('KK phase'), axis off
subplot(3,3,6), imagesc(log10(abs(kk_sample_field_Fourier)),[-
4,max(log10(abs(kk_sample_field_Fourier(:))))]), axis image,
colorbar, title('Fourier spectrum (log_1_0)'), axis off
% subplot(3,3,6), imagesc((abs(kk_sample_field_Fourier))), axis
image, colorbar, title('Fourier spectrum'), axis off

subplot(3,3,7),
imagesc(abs(ox_sample_field),[0,max(abs(ox_sample_field(:)))]),
axis image, colorbar, title('off-axis amplitude'), axis off
subplot(3,3,8), imagesc((angle(ox_sample_field)),[-pi,pi]), axis
image, colorbar, title('off-axis phase'), axis off
subplot(3,3,9), imagesc(log10(abs(ox_sample_field_Fourier)),[-
4,max(log10(abs(ox_sample_field_Fourier(:))))]), axis image,
colorbar, title('Fourier spectrum (log_1_0)'), axis off
% subplot(3,3,9), imagesc((abs(ox_sample_field_Fourier))), axis
image, colorbar, title('Fourier spectrum'), axis off

% Calculate g(1) correlation with the solution
g1_corr_kk = corrcoef(kk_sample_field(:),sample_field(:));
disp(['KK method, g(1) correlation = ',
num2str(abs(g1_corr_kk(1,2)))])

g1_corr_ox = corrcoef(ox_sample_field(:),sample_field(:));
disp(['off-axis method, g(1) correlation = ',
num2str(abs(g1_corr_ox(1,2)))])
```

References

1. J. P. Havlicek, J. W. Havlicek, and A. C. Bovik, "The analytic image," in *Image Processing, 1997. Proceedings., International Conference on*, (IEEE, 1997), 446-449.
2. C. E. Shannon, "Communication in the presence of noise," Proceedings of the IRE **37**, 10-21 (1949).
3. E. T. Whittaker, "XVIII.—On the functions which are represented by the expansions of the interpolation-theory," Proceedings of the Royal Society of Edinburgh **35**, 181-194 (1915).
4. S. L. Marple, "Computing the discrete-time "analytic" signal via FFT," Ieee Transactions on Signal Processing **47**, 2600-2603 (1999).
5. T. Colomb, J. Kuhn, F. Charriere, C. Depeursinge, P. Marquet, and N. Aspert, "Total aberrations compensation in digital holographic microscopy with a reference conjugated hologram," Opt Express **14**, 4300-4306 (2006).